40 cy
5/12/65

~~CONFIDENTIAL~~

MASTER

LA-3214-MS

AEC RESEARCH AND DEVELOPMENT REPORT

UNCLASSIFIED

LOS ALAMOS SCIENTIFIC LABORATORY
OF THE UNIVERSITY OF CALIFORNIA ○ LOS ALAMOS NEW MEXICO

PARTICLE SIZE DISTRIBUTION FROM A ONE-NINTH-SCALE ROVER REACTOR AXIAL-HE DESTRUCT

(Title Unclassified)

This document contains Confidential Restricted Data relating to civilian applications of atomic energy.

~~RESTRICTED DATA~~

This document contains restricted data as defined in the Atomic Energy Act of 1954. Its transmittal or the disclosure of its contents in any manner to an unauthorized person is prohibited.

~~CONFIDENTIAL~~

DISCLAIMER

Printed in USA. Charge $1.05. Available from the U.S. Atomic Energy Commission, Technical Information Service Extension, P. O. Box 1001, Oak Ridge, Tennessee. Please direct to the same address inquiries covering the procurement of other classified AEC reports.

~~CONFIDENTIAL~~

UNCLASSIFIED

LA-3214-MS
C-91, NUCLEAR REACTORS
FOR ROCKET PROPULSION
M-3679 (38th Ed.)

38a 0000

LOS ALAMOS SCIENTIFIC LABORATORY
OF THE UNIVERSITY OF CALIFORNIA LOS ALAMOS NEW MEXICO

REPORT WRITTEN: December 15, 1964

REPORT DISTRIBUTED: April 2, 1965

PARTICLE SIZE DISTRIBUTION FROM A ONE-NINTH-SCALE ROVER REACTOR AXIAL-HE DESTRUCT

(Title Unclassified)

Work done by:

Evan E. Campbell
Harold M. Ide
William D. Moss

Report written by:

Evan E. Campbell
William D. Moss

Contract W-7405-ENG. 36 with the U. S. Atomic Energy Commission

~~RESTRICTED DATA~~

~~CONFIDENTIAL~~

BLANK

Abstract

Thirty-three Rover type fuel elements, representing a scaled down volume of a Kiwi reactor, weighed 2955.5 g and were fragmented by 49 g of high explosives. The particle size distribution and particle characteristics were determined. The mass median particle diameter was 1125 μ. One-third of all beaded fuel was freed as individual uranium carbide beads. Various methods of analysis and interpretation are given.

BLANK

Preface

The test was requested by SNPO-Washington as an adjunct to the Kiwi-TNT test. At the request of L. D. P. King, Rover Flight Safety Director, a destructive test of a one-ninth-scale Rover reactor assembly was carried out by Jerry Wackerly of Group GMX-7. The collection and sizing of the debris were carried out by the Health Division in order to gain experience and develop techniques applicable to the forthcoming Kiwi-TNT test. Because of the health problems associated with the core disposal program, the Health Division facilities were made available through Group H-5.

BLANK

Contents

	Page
Abstract	3
Preface	5
Introduction	9
Core Disposal	10
Debris Recovery	10
Chamber	10
Observations at the Time of the Explosion	11
Floor	11
Recovery (Weight of the Debris in Grams)	11
Polyethylene Ground Cover	12
Wall	12
Particle Size Study	13
Sieve Analysis	13
Microscopy	14
Distribution of Beads	19
Surface Character of Particles	21
Density	23
Individual Particle Density	24
Particle Size as a Function of Radial Distance from the Explosive	24
Summary	25
Conclusions - Technical Applicability to the Kiwi-TNT Tests	26
Appendix - Comparison with Other Tests	28

Tables

1.	Sieve Analysis and Physical Data on Selected Random Sample	30
2.	Sieve Analysis and Physical Data on Reactor Debris	31

Figures

		Page
1.	Pre-shot assembly	32
2.	Chamber immediately after detonation	33
3.	Debris from floor of chamber	34
4.	Random sample	35
5.	Plastic ground cover	36
6.	Styrofoam batten showing impaction by particles	37
7.	Path of fragment through Styrofoam	38
8.	Mass particle size distribution. 285 g sample	39
9.	Mass particle size distribution. 1864 g sample	40
10.	Particle distribution of each sieve fraction	41
11.	Distribution of particle dimensions. Particles > 5000 μ	42
12.	Weight of single particle vs. measured diameter	43
13.	Number of particles in each sieve range	44
14.	Size distribution by number of particles	45
15.	Particle distribution by volume	46
16.	Distribution of uranium by particle size fractions	47
17.	Surface characteristics of a particle	48
18.	Sieved sample. 125 to 177 μ	49
19.	Sieved sample. 88 to 125 μ	50
20.	Particle size distribution	51

Introduction

A one-ninth-scale Rover reactor fuel assembly was destroyed by a non-nuclear deliberate explosion in order to determine core dispersal. The present knowledge of core disposal systems has been limited to the disassembly of the core by High Explosives (HE) and may be entirely different in character and result from that generated by a nuclear excursion. Because of the difference between energy dispersion, timing, and location, the primary factors considered in this report are: degree of bead knockout, change in particle size distribution with respect to the beaded elements, and problems associated with particle sizing.

Other than comparison, no effort has been made to relate these findings with previous studies or make any interpretation as applied to those problems associated with a destruct mechanism of this nature in space.

Core Disposal

Thirty-three Rover type fuel rods (elements), 7 in. long, were packaged as described in LA-2688. The unit weighed 2955.5 g and was fragmented by an axial explosive consisting of 49 g of Comp. "C" and 4 g of detonator. The assembly was placed on a 10-in.-square aluminum reflector mounted on an aluminum stand 6 in. from the floor of a 4 by 4 by 4 ft open-top detonation chamber (Fig. 1).

Three rings of the hexagonal elements were placed around an axial explosive. The 6 elements immediately concentric to the explosive were painted red, the next 12 were painted blue, and the 12 whole and 6 half elements were painted yellow. The unit was held together with five rubber bands and wrapping of 1-in. masking tape at the top and bottom.

Debris Recovery

Chamber. The detonation chamber was open at the top and the walls covered with sheets of $\frac{1}{4}$-in.-thick black neoprene on the bottom and three walls. The fourth wall was covered with three sheets of 4-in.-thick Styrofoam. A sheet of polyethylene 1/32 in. thick was placed over the Styrofoam to prevent excessive surface damage at the time of the explosion. Polyethylene sheets were placed on the ground around the chamber, extending 4 ft from the lip of the chamber.

Observations at the Time of the Explosion. Approximately 30 sec after the detonation, the cloud from the explosion had risen 30 to 50 ft and moved to a distance of 50 to 75 ft from ground zero. The cloud was dark but not black and only extremely fine particulates appeared to be present. The cloud dissipated within 200 ft with a mild breeze. No effort was made to characterize the particle distribution within the cloud. Figure 2 shows the chamber immediately after the detonation; note the bottom sheet of Styrofoam still in place while the upper two sheets have fallen to the floor along with one neoprene sheet.

Floor. The debris on the floor of the chamber was carefully swept into glass jars for analysis (Fig. 3). A small portion of the debris was removed from the floor as a random sample (Fig. 4). The purpose of this selection was to analyze the sample separately and determine the need for a complete or extensive analysis of the total amount of debris recovered.

Recovery (Weight of the Debris in Grams).

Vacuumed from walls and polyethylene ..	~ 685.0
Swept from floor as total sample ..	1864.0
Random sample from floor ..	28.937
Debris collected from Styrofoam ..	265.28

Estimation of suspended particles in solution from the dissolution of the Styrofoam	.. 15.0
Weight of debris recovered	.. 2858.21
	~ 97% recovery

Polyethylene Ground Cover. This was rolled up for cleaning in the laboratory. The ground cover (Fig. 5) was swept with a camel's hair brush and all particles dusted into a glass container for analysis. Recognizable sticks, rocks, and extraneous metal objects were removed. Particle size distribution was not attempted on such a small sample; however, in general there were less fines and the large particles were not as large as the general sample.

Wall. The rubber-lined walls were vacuumed free of particulates using a special high volume vacuum (Staplex high volume air sampler) with a cyclone separator and ultra filter. The velocity of the particulates in the hose and cyclone caused a sufficient amount of size degradation so that only the mass recovery was determined.

The Styrofoam wall was badly damaged. Figure 6 shows the effect of the particulates after impaction.

The polyethylene was vacuumed as above and the particles recovered for weight only. The Styrofoam blocks and the paths made in them by particles (Fig. 7) were examined,

and several particles were cut out. The particles were observed under stereo microscopy for greater detail. Some of the paths were heavily laden with small particles, indicating that the particles fell into the hole after the larger particle, or abraded from the surface of the large particle. Beads and fragments of graphite are clearly visible in Fig. 7.

The Styrofoam blocks were dissolved in toluene and diluted with methyl chloroform; the viscosity of the solution made it impractical to establish a precise size distribution. The distribution of the particles recovered from the dissolution of the Styrofoam had a mass median diameter of 2700 μ, determined by a standard sieve set and the log median sieve size. The weight of debris recovered from the Styrofoam was 280 g, assuming 15 g of fines were lost in the solution.

Particle Size Study

Sieve Analysis. The individual masses of particles were carefully sieved in a series of Tyler sieves. The assumed friability of the particles precluded the standard Ro-tap or shaking processes. The sieves were assembled and taped to prevent loss and external surface contamination. The sieves were then shaken for 1 hour without vigorous bumping or extreme agitation. Each sieve fraction was weighed and an aliquot taken for particle size distribution

measurements, uranium activity measurements, particle density determination, and special characteristic studies. Each sieve fraction was used to obtain the particle distribution shown on Figs. 8 and 9, using the screen range of particle size as the abscissa and the cumulative per cent of each fraction as an ordinate plotted on log probability paper. The data are shown on Tables 1 and 2 along with other pertinent information from the two samples. A series of calibrated glass beads was introduced into the same set of sieves used in this study. The size distribution on each sieve fraction confirmed the separation found in these experiments. There appears to be no significant difference between the gross or 1864 g sample and the random 28.5 g sample. Coning and quartering would produce a statistically more valid sample, but the difference is sufficiently small to warrant small sample techniques.

Microscopy. Aliquots of each of the sieved samples were spread dry on a microscope slide and several photographs taken of each fraction. The photographs were taken at various magnifications, employing a stage micrometer or ruler for calibration, using both 35 mm and 4 by 5 in. film. Examples of these are shown in the composite Fig. 10. The particles were then sized using a Zeiss particle size counter based on the diameter of a circle of equal area.

The distribution of the particles greater than 2.5 mm was determined by manual counting and the determination of the product of the longest dimension times the shortest dimension, and calculating the diameter of an equal area circle.

Figure 11 illustrates the distribution of the particle shape of these particulates by plotting the longest and smallest dimensions. The irregular shape of the long dimension curve is caused by the randomness of the fracturing length, while the shortest dimension usually is some multiple of 2 mm which corresponds to the thin wall between the longitudinal drill holes in the fuel element. Most of the particles had one dimension that was less than one half the smallest of the other two dimensions and presented themselves as being smaller than the volume calculated from the observed diameter would indicate. Observation of several particles in each fraction confirmed that the irregular dimension illustrated for the larger particles was true throughout most of the sieve fraction. The mass median particle diameter was found by sieve analysis to be between 1000 and 1400 μ. Using the log mean of the sieve range the mass median diameter is 1125 μ. Because of the type of agitation used for the sieve analysis, some of the finer particles were not completely removed from each of the

sieve fractions. The reliability of each sieve fraction is illustrated by the actual photographic count distribution on each of the sieve fractions (Fig. 9). The fine particles in each fraction could bias the count distribution; however, these fines contribute very little to the weight of each fraction or even the total sample.

In order to determine or predict the number of particles which may be expected, two methods of analysis were used. In the first method, 100 particles of each of the sieves were weighed, and the weight per particle size range or log median sieve size was plotted on log-log paper (Fig. 12). The 125 μ particle was the smallest particle that could be weighed with reliability. The data are shown on Table 1. The weight per particle of each size range was then corrected to a linear relationship maintaining a constant size; from this it was then possible to assign an average weight per particle in a size range or sieve fraction. Using the weight recovered on each sieve, it was then possible to convert to a number of particles per sieve range which yields a line with a slope of approximately 0.5. These data are shown on Fig. 13. The non-linearity is most noticeable between 1000 and 10,000 μ; and the particle size overlap, particularly in the smaller sieve size range, accounts for some of the discrepancies in the lower fraction.

To establish the particle size distribution, it was necessary to determine a composite distribution curve of the entire debris collected. The observed overlap of particles in the size distribution by count sieve fraction from one to another required the summation of the number of particles overlapping between several sieve ranges. The per cent of particles in each particle size range by count (illustrated in Fig. 9) was used to obtain the count distribution in the overlap area, which was multiplied by the number of particles on the given sieve. These were added and a cumulative distribution curve calculated and constructed as shown in Fig. 14, Curve #2. It will be noted that the slope of that portion of the curve below 20 μ is identical to the less than 44 μ fraction based on count from Fig. 9. The influence of the number of particles in this sieve section is so great that the entire curve is biased. By plotting all of the data the count median particle diameter is 9.2 μ. However, if it is assumed that all particles less than 15 μ are of little or no interest, and the data corrected for this exclusion, the count median diameter would become 150 μ; 15 μ also represents the knee of the curve. In either case, the 100 μ range must be included because of the presence of the beads and/or bead fragments in the debris.

Another method of data presentation employs the particle volume concept. The particle size distribution by count on each sieve (Fig. 9) is transformed by the Hatch and Choate equation ($\log Mg' = \log Mg + 6.91 \log^2\sigma_g$) to a distribution by volume on each sieve illustrated by the family of lines on Fig. 15. Since the density varies somewhat with the size, a series of size ranges was set up starting at 10 μ with the upper limit of each size range being $\sqrt{2}$ times the lower limit. The percentage volume in each size range for each sieve is then divided by the average density for that sieve and multiplied by the total weight on the corresponding sieve. This gives the weight of material on each sieve in each size range. These are then summed for each size range and divided by the total mass of the sample to give the particle size distribution by mass. The cumulative form of this distribution is shown on Fig. 15. The mass median diameter of this distribution is approximately 2000 μ.

The particle size distribution by number for the total sample may now be obtained by proceeding in the reverse manner, weighting the per cent in each size range by the reciprocal of the cube of the diameter. The result is given as Curve #3 in Fig. 14 and yields a count median diameter of 9.7 μ. The unusual agreement between this

method and the previous method probably is more fortuitous than either method warrants.

Distribution of Beads. The extent of bead loss (bead knockout) during fracturing was determined by a relative method of analysis. Twenty-five grams of each of the particle size fractions were carefully weighed and the gamma activity determined in a gamma spectrometer. The sample fraction and a uranyl nitrate reference standard were counted under similar geometry. The activity contributed by thorium-234 and protactinium-234 was related to the uranium content. Even though the analysis was not meant to be absolute, it serves as a comparison of uranium activity in each of the sieved fractions. The data are shown in Table 2 and illustrated in Fig. 16. The amount of uranium per gram (Histogram #1) in each particle size fraction is variable, showing a gradual loss of uranium from 2500 to 177 μ. The loss of uranium, as beads, is recovered in the particle size range from 88 to 177 μ. Less than 0.4% of the weight in the fraction less than 88 μ is contributed by uranium sorbed on graphite and not to whole beads. The fragments in this particle size range do not appear spherical, and the observed uranium content probably is associated with the pyrographitization process and subsequent abrasion rather than degradation of the beads to finer particle sizes during the destruct test or sieving.

If the matrix had been homogeneous, the concentration of uranium per gram in all of the particle size fractions would be constant at about 0.15 g of uranium per gram of sample (Curve #1). This value is the average of the original system before destruct. Superimposed on the graph is a histogram of a typical bead mixture where the mean particle size is 98 μ, showing that less than 0.4% of the beads could be found in the sieved fractions below 78 μ. If the cladding were lost from the free beads, they would be found in the particle size range from 77 to 125 μ. Any adsorbed matrix would shift the distribution to the right or to a larger particle size. A typical bead distribution prior to graphitization is shown below:

Typical Particle Size Distribution of Beads Prior to Graphitization

Diameter (μ)	Per Cent
65	0.3
80	14.6
100	57.3
115	31.0
150	11.4
170	0.2
X's	0.1

Histogram #2 on Fig. 16 (particle size range vs. grams of uranium per sample) illustrates an increase of uranium

in particle sizes from 88 to 450 μ. If the matrix were homogeneous or there were no loss of beads at the fractured surfaces, the uranium content per sample would follow a slight curve (Curve #2) drawn through the histogram to about 100 μ. The loss of beads from the fractured surface is illustrated by the increase in the uranium content of the fraction from 88 to 450 μ. Less than 0.005 g of uranium per gram of sample was found below 88 μ, confirming the absence of beads or bead fragments.

No evidence of broken beads was found in the destruct data presented; however, they were freed from the fractured surfaces with and without attached matrix. Since the amount of uranium by unit weight is only slightly increased in the bead size, it shows that the number of beads to grams of graphite remains relatively constant.

Surface Character of Particles. With the aid of a stereo microscope, the surface of several particles was examined for general characteristics. A typical illustration is shown in Fig. 17 with observations listed below:

1. The beads were seldom dislodged alone but carried varying amounts of graphite matrix attached to their surfaces. No well-defined bead pits are seen.

2. Clearly indentifiable beads were visible on the fractured surface; approximately 32% of the number of beads

that should be present in a given area are identifiable (see A of Fig. 17). The bead knockout factor of approximately one third of the beads per unit area allows them to be degraded as individual particles.

3. All particles recognizable as having a definite shape, greater than 500 μ, appear to have been broken longitudinally with the drill holes.

4. The niobium cladding crenates under pressure and produces a rather uniform particle size when degraded to particles less than 100 μ. Particles less than this size usually do not exhibit any niobium adsorbed to any of their surfaces.

5. Large numbers of small particles less than 100 μ are clearly visible adsorbed to the niobium coating, illustrated by B in Fig. 17. Vigorous sieve shaking would have removed these particles and yet, at the same time, polished the larger particles, yielding an even more biased result.

The two sieved samples illustrated in Figs. 18 and 19 are the fractions from 125 to 177 μ and 88 to 125 μ, respectively. The long flat particle in the center of Fig.18 has a typical surface referred to before as the crenated niobium coating. The brassy surface is divided into a large number of scale-like particles which are less than 50 μ. This scale is lost from the surface of the particle as

degradation occurs and results in a concentration of niobium in the size range of less than 88 μ. There was an abundance of these brassy particles in the less than 44 μ fraction. Beads of approximately 125 to 177 μ were clearly identifiable in this range. These beads appear to be coated and often contain small portions of graphite matrix attached to their surfaces, causing an irregular shape and larger particle size than a free cladded bead.

One of the many half shells or shell fragments visible in the 88 to 125 μ sieve range is shown at the upper right of Fig. 19. In addition to the graphite shells, the beads themselves are clearly identifiable as unclad beads of approximately 100 μ diameter.

Density

The methods for the determination of density in particles is of little value for the graphite used in this study. The compacted density contains errors introduced by the inability of the solvent to penetrate completely all of the interstitial spaces. The particles are not easily wettable, consequently ethanol was used as the supporting liquid for pycnometric measurements. The data are shown in Table 1. The density of the particles down to 177 μ should approximate the original density of the matrix used in this experiment. Those fractions below this size should

show an increase in density if a large number of free beads were present. A slight increase in density is observed; however, as pointed out earlier, the uranium to graphite ratio by weight in each sample appears to be relatively constant. The somewhat higher density of the less than 44 μ fraction is caused by the abundance of niobium carbide and not uranium carbide.

Individual Particle Density. One hundred particles of each fraction down to 125 μ were counted and weighed. The weight of a single particle is shown in Table 1. Assuming that the particle size is representative of a sphere, which is not true, the density of each particle closely approximates one.

Particle Size as a Function of Radial Distance from the Explosive. Even though the elements were painted different colors, it was not practical to size the debris with respect to these colors. Using fluorescence microscopy and visual fluorescence, the red paint was detected on particles in all size ranges; however, the frequency on large particles was much less than either the blue or the yellow particles. The blue painted elements lost the surface color easily. Qualitatively, as might be expected, those elements closer to the explosion broke into smaller particles than the peripheral elements.

Summary

Under the conditions of this single experiment, the Rover 202 fuel element disposal would create the following particle systems:

1. The mass median particle diameter of the fragments would be 1125 μ based on sieve analysis.

2. Ten per cent by weight of the reactor debris has a diameter of less than 100 μ.

3. Forty per cent by weight of the reactor debris has a diameter of greater than 2500 μ or 0.1 in.

4. Count median diameter of the particles is 9 μ confirmed by particle weight to be 9.2 μ.

5. Approximately one-third of all beads at the fractured surface are free to become degraded to individual beads.

6. In the 44 to 88 μ range, 4.7% of the particles are free, unclad beads and 8% of the particles are shells or shell fragments.

7. In the 88 to 125 μ range, 5.4% of the particles are free beads and approximately 2% are shell or shell fragments; the remainder are graphite-coated beads.

8. Thirty per cent of the particles in the 125 to 177 μ range are beads containing small amounts of attached graphite matrix; the remainder are graphite or graphite-encased bead fragments.

9. The shape of the particles is primarily irregular parallelepipeds broken along the axis of the drill holes.

10. The niobium lining becomes crenated and detached forming particles less than 125 μ primarily concentrated in the 44 to 88 μ range.

11. The friability of the particles and the detonation chamber confinement may have produced a smaller mass median particle size than a free dispersal destruct test. This was suggested by the Styrofoam trap particle size distribution which has a mass median particle diameter of 2700 μ which does not include many of the fines that were held on the polyethylene.

12. Prolonged mechanical shaking in a Ro-tap-type sieve separator produced polished particles which showed no rough edges and only had a small effect on the mass median particle size.

Conclusions - Technical Applicability to the Kiwi-TNT Tests

1. Sieve analysis of nuclear exploded fuel elements will determine mass distribution, depending on the friability of the particles.

2. The bleeding of uranium from the beads to the interstitial spaces of the pyrographite shell and the graphite matrix because of high temperature will increase the fission product concentration in the particle fractions less than 100 μ.

3. Individual particle characterization will become more important because of the diffusion of the uranium and fission products from the beads into the graphite resulting in a radioactive particle in the particle size range less than 100 μ.

4. The particle size cannot be predicted for the Kiwi-TNT test.

5. Radiometric sizing of the particles at early times after the nuclear destruct test will be of value for the smaller particles (< 100 μ).

6. Radiometric studies of individual and groups of particles vs. distance from the test pad is necessary in order to evaluate mean particle size by count and reconstruct the reactor core by mass.

7. Density measurements will be of little value in the interpretation of the particle character.

8. No effort should be made to determine the radioactivity of all of the samples; only a selected few should be rigorously analyzed for radioactivity and decay, and qualitative gamma spectra taken.

9. Based on the samples from #8 above and the analysis of the samples for uranium and barium-lanthanum determined at some weeks after the test, all samples can be subjected to radiometric interpretation and extrapolated back to some finite time after detonation.

Appendix - Comparison with Other Tests

The particle size data accumulated by Group H-5 from a test conducted by Group GMX-11 are compared with previous tests. The following quotation is taken from NUS-167 by Ralph S. Decker of the Space Nuclear Propulsion Office of the USAEC: "A major factor in estimation of inner reaction probabilities and effects is contributed by the particle size distribution assumption. The distribution assumed to result from destruct action determines the extent of aerial coverage, the activity concentration, the delay in re-entry and the dose route themselves. The most pertinent data available to date are those deriving from the APG-2 destruct tests, conducted at the Aberdeen Proving Grounds using depleted fuel elements. Unfortunately, no differentiation was made of size distribution in the range less than 1/32 of an inch which provides the particles most important from an internal and skin dose viewpoint, and which in these tests constituted some 50 +% of the core material. Similarly, the LMSC treatment of particle re-entry neglected this class, making necessary extrapolations which are described below."

The LASL one-ninth-scale Rover reactor assembly test did include all particles less than 40 μ. This information is presented on Fig. 20 along with particle size distribution information from Mr. Decker. Our data, as diamonds, closely approximate the APG-2 data, circles, and show that the distribution of particles less than 1000 μ lies between the Decker-assumed data and the selected distribution data. The inflection observed below 88 μ is taken from volume and count distribution rather than from observed mass.

The mass distribution of large particles from this study also compares favorably with the data presented by Wackerly in LAMS-2688.

TABLE NO. 1 - SIEVE ANALYSIS AND PHYSICAL DATA ON SELECTED RANDOM SAMPLE (Wt. 28.9 g)

Sieve Range (Numbers)	Sieve Range in (μ)	Wt. of Sieve Sample (g)	Cumulative % of Fraction	Mean Particle Diam. by Count (μ)	No. of Particle Per Sample	Avg. Wt. of One of 100 Particles (g X 10^{-5})	Density (g/cm^3)
Hand Measured	>10,000	2.4640	100	--	3	82100	
Hand Measured	5,000 - 10,000	2.4983	91.49	--	91	5960	
Hand Measured	2,500 - 5,000	6.6637	68.49	3000	73	2787	
>12	1,651 - 2,500	4.5629	59.86	2150	412	1108	2.235
12 - 16	1,168 - 1,651	2.5319	44.11	1600	599	422.9	2.251
16 - 20	840 - 1,168	1.9601	35.36	1020	1511	129.7	2.278
20 - 32	495 - 840	1.4328	28.59	700	8727	21.3	2.095
32 - 80	177 - 495	2.7129	23.65	200	29812	9.1	2.02
80 - 120	125 - 177	1.1940	14.28	150	79600	1.5	2.774
120 - 170	88 - 125	0.6538	10.16	108	-----	---	3.549
170 - 325	44 - 88	1.3125	7.9	----	-----		2.819
325 - 400)	<44	0.9768	3.37	----	-----		3.296
<400)		28.937 (Total)					

CONFIDENTIAL

TABLE NO. 2 - SIEVE ANALYSIS AND PHYSICAL DATA ON REACTOR DEBRIS (Wt. 1864 g)

Sieve Range (Numbers)	Sieve Range in (μ)	Wt. of Sieve Sample (g)	Cumulative % of Fraction	Mean Particle Diam. by Count (μ)	Sigma 84%/50%	Count/ Mass Ratio	Mean Volume Diam.	g U/g Sample	g of U/ Sample
<4	5000	86.0	100	7800	1.30	1.25	9750	0.1312	11.25
4 - 8	2500 - 5000	438.0	95.38	3500	1.47	1.55	5430	0.1391	60.9
8 -12	1651 - 2500	273.0	71.88	2200	1.17	1.1	2420	0.1585	43.2
12 -16	1160 - 1651	212.0	57.24	1500	1.14	1.1	1650	0.1385	29.2
16 -20	840 - 1160	143.5	45.86	1160	1.15	1.1	1275	0.1292	18.5
20 -32	495 - 840	137.0	38.14	760	1.36	1.3	987	0.1187	16.25
32 -80	177 - 495	192.0	29.90	260	1.42	1.45	377	0.1187	23.8
80 -120	125 - 177	157.0	20.50	170	1.2	1.13	192	0.2470	19.6
120 -170	88 - 125	67.0	12.10	122	1.3	1.25	153	0.1723	11.5
170 -325	44 - 88	100.5	8.5	75	1.25	1.18	88.5	0.0404	4.04
325 -400	<44	58.0 (30.8	3.1	3.1	9.2	1.63	2.0	18.4	0.00833	0.483
<400		(27.2		1.45				(Aver) 0.127445	238.77 gms recovered

Total 1864

CONFIDENTIAL

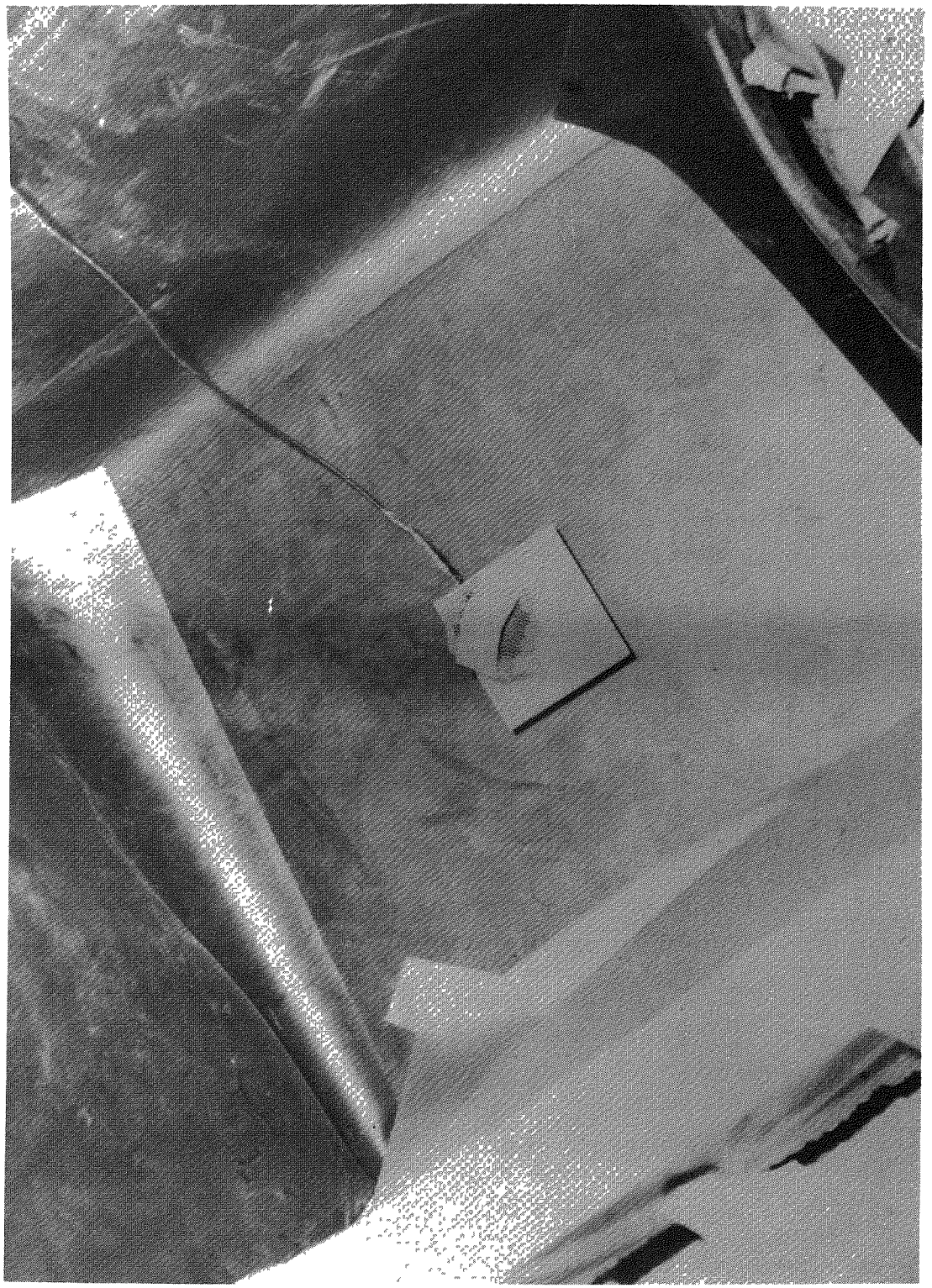

Fig. 1. Pre-shot assembly.

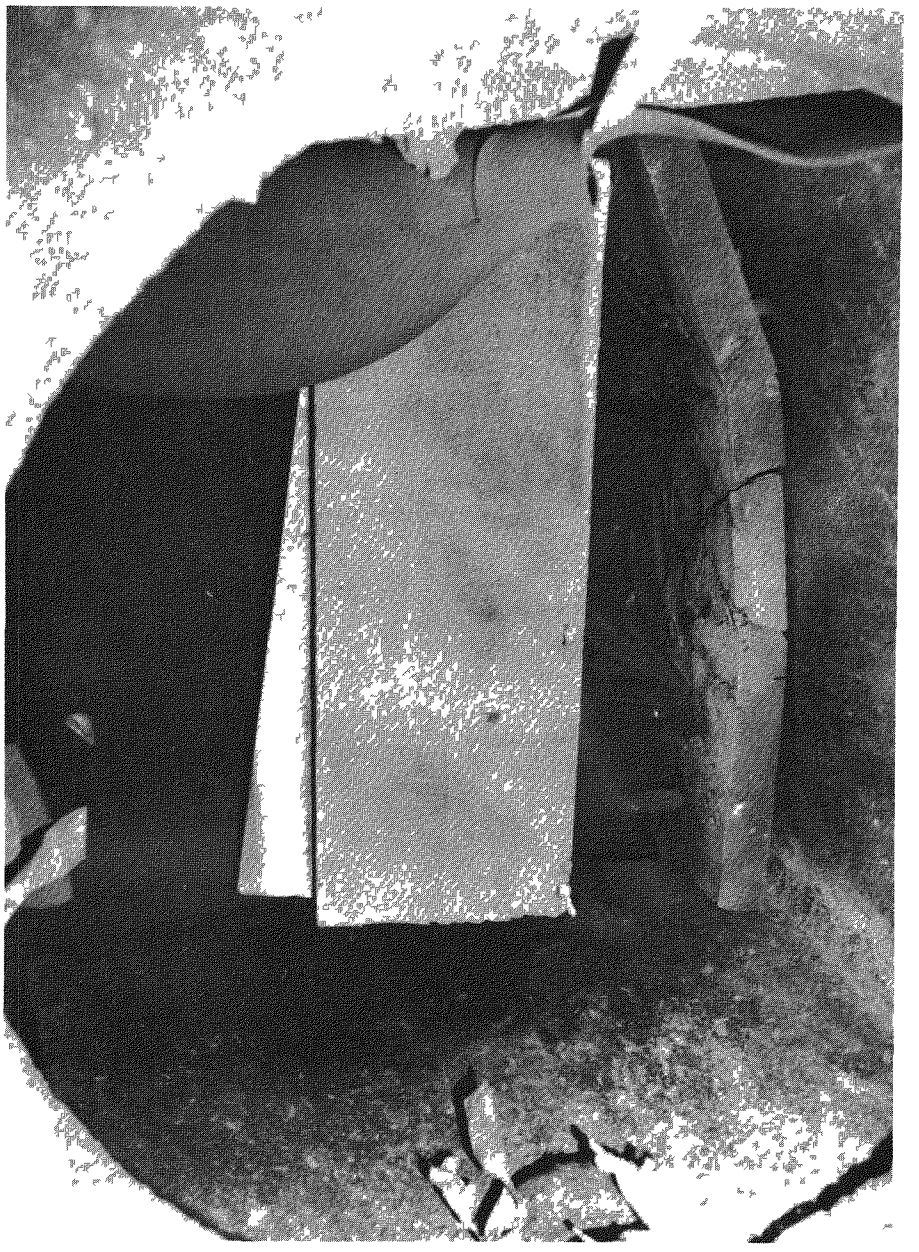

Fig. 2. Chamber immediately after detonation.

Fig. 3. Debris from floor of chamber.

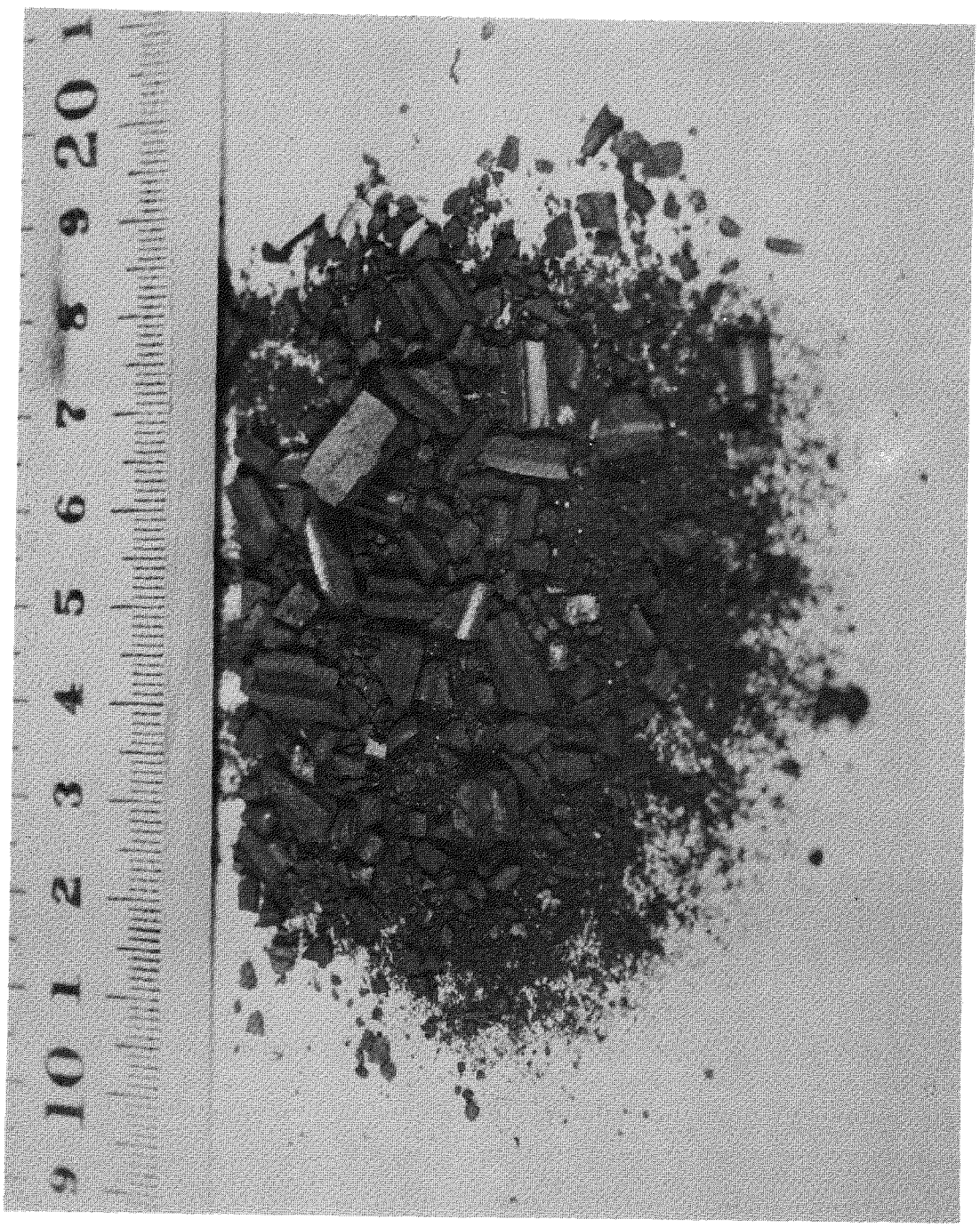

Fig. 4. Random sample.

Fig. 5. Plastic ground cover.

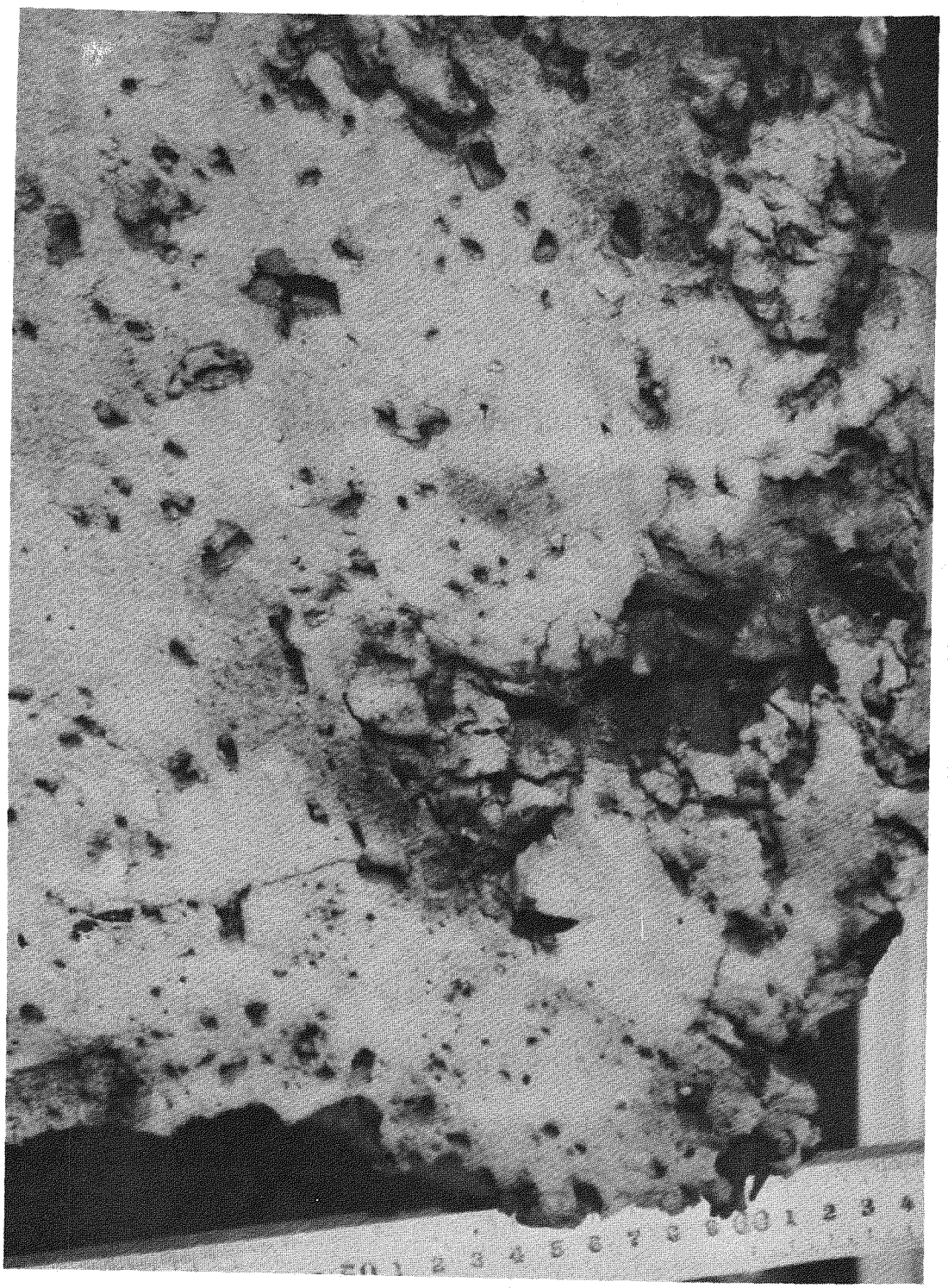

Fig. 6. Styrofoam batten showing impaction by particles.

Fig. 7. Path of fragment through Styrofoam.

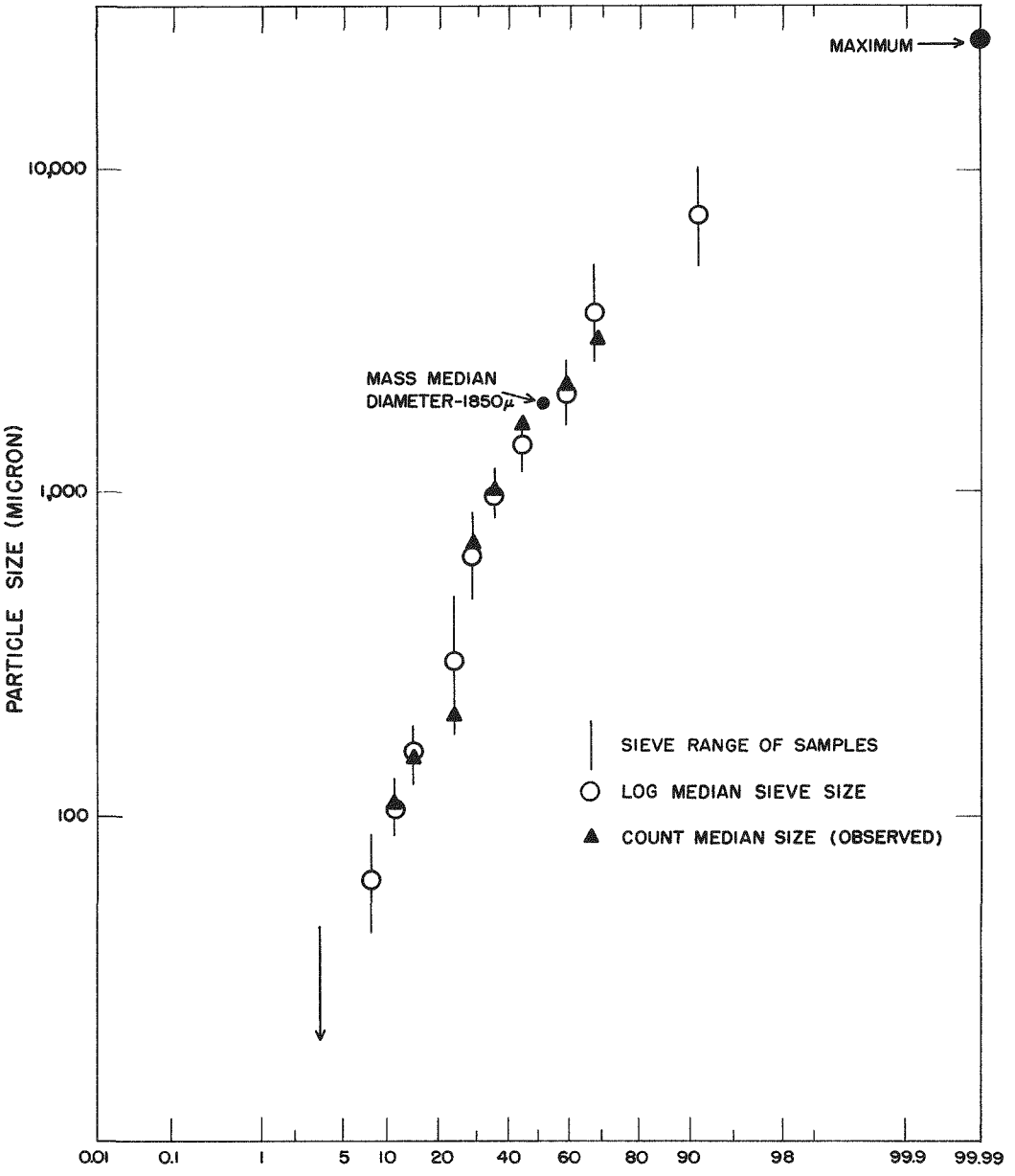

Fig. 8. Mass particle size distribution. 285 g sample.

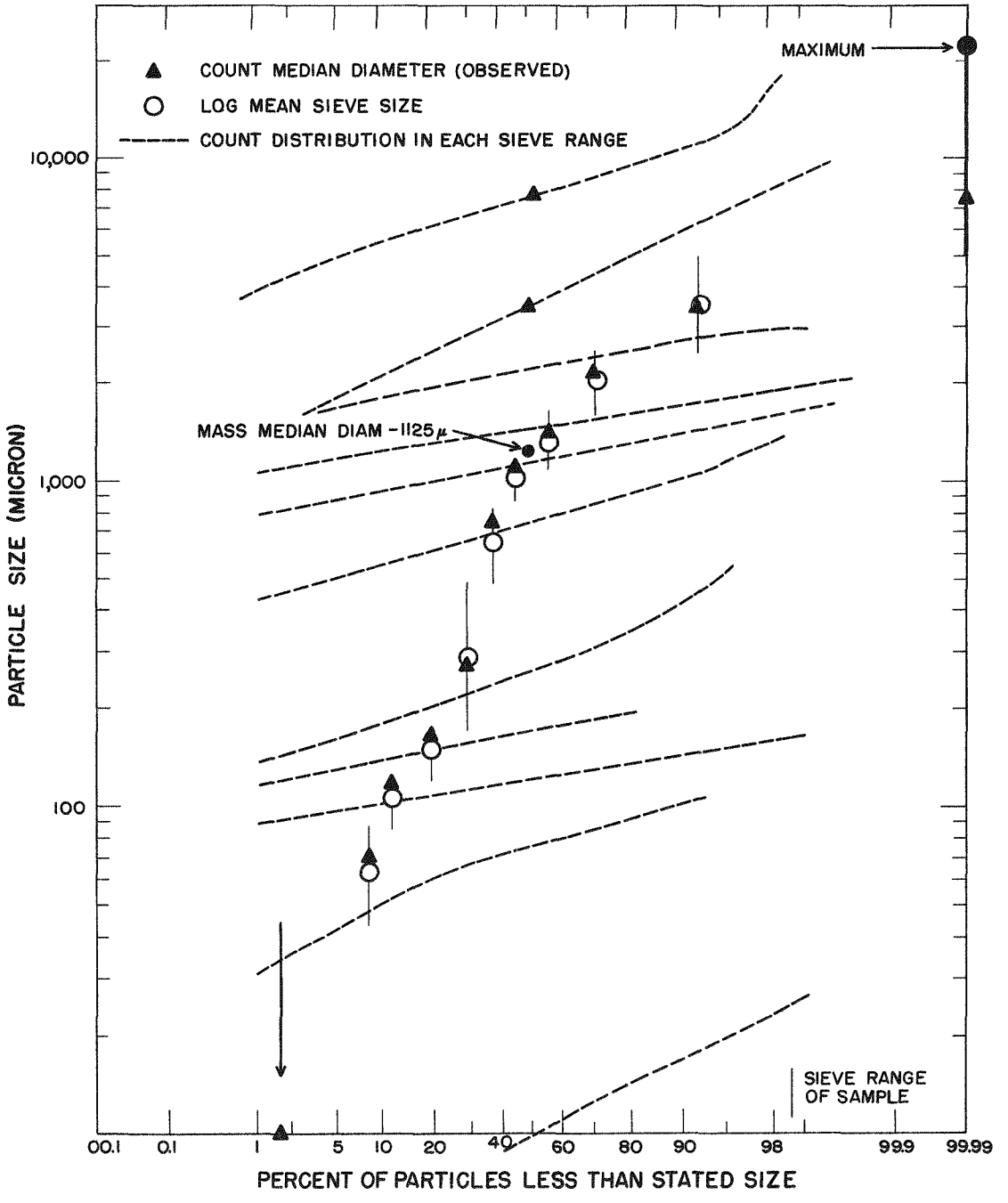

Fig. 9. Mass particle size distribution. 1864 g sample.

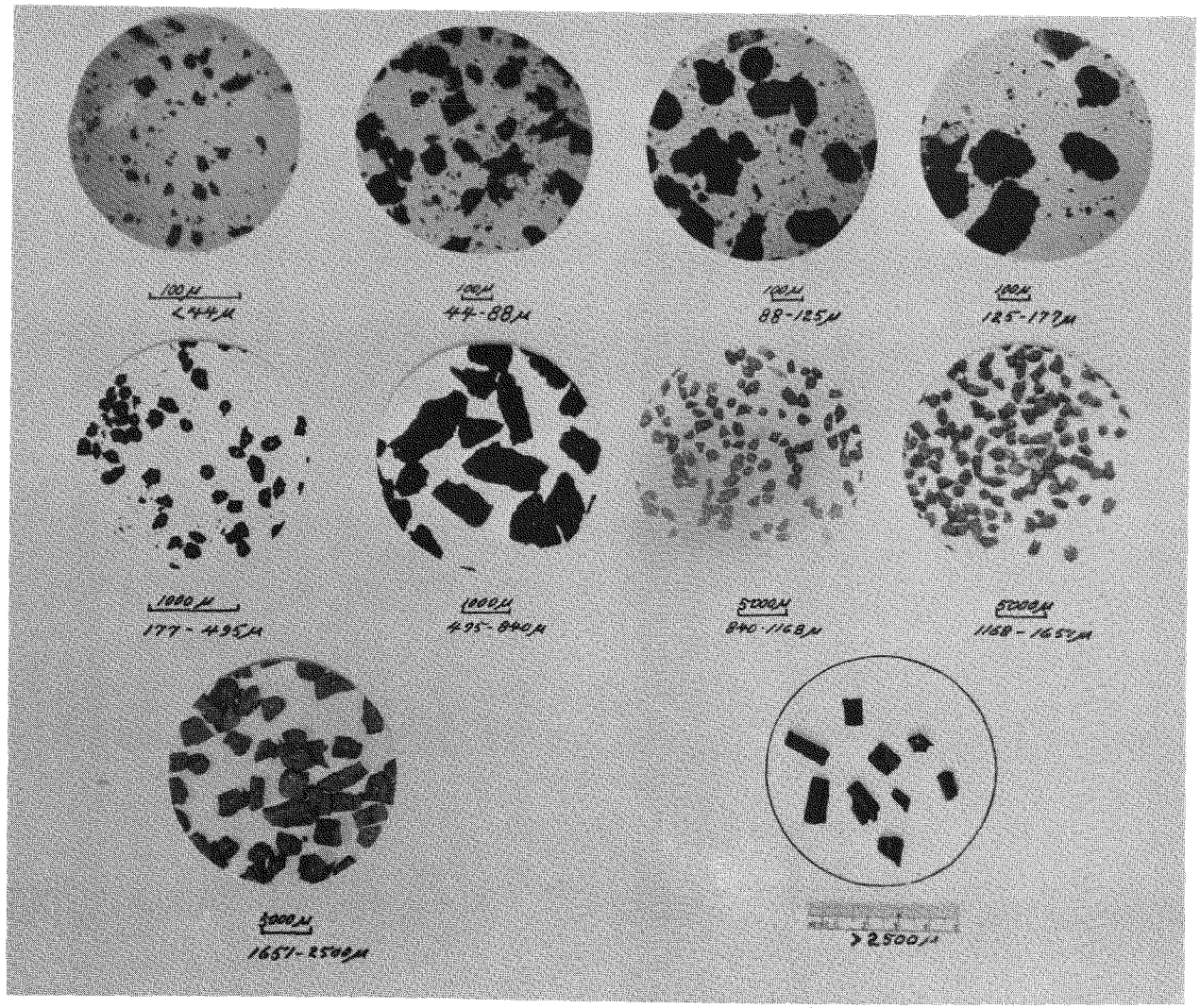

Fig. 10. Particle distribution of each sieve fraction.

CONFIDENTIAL

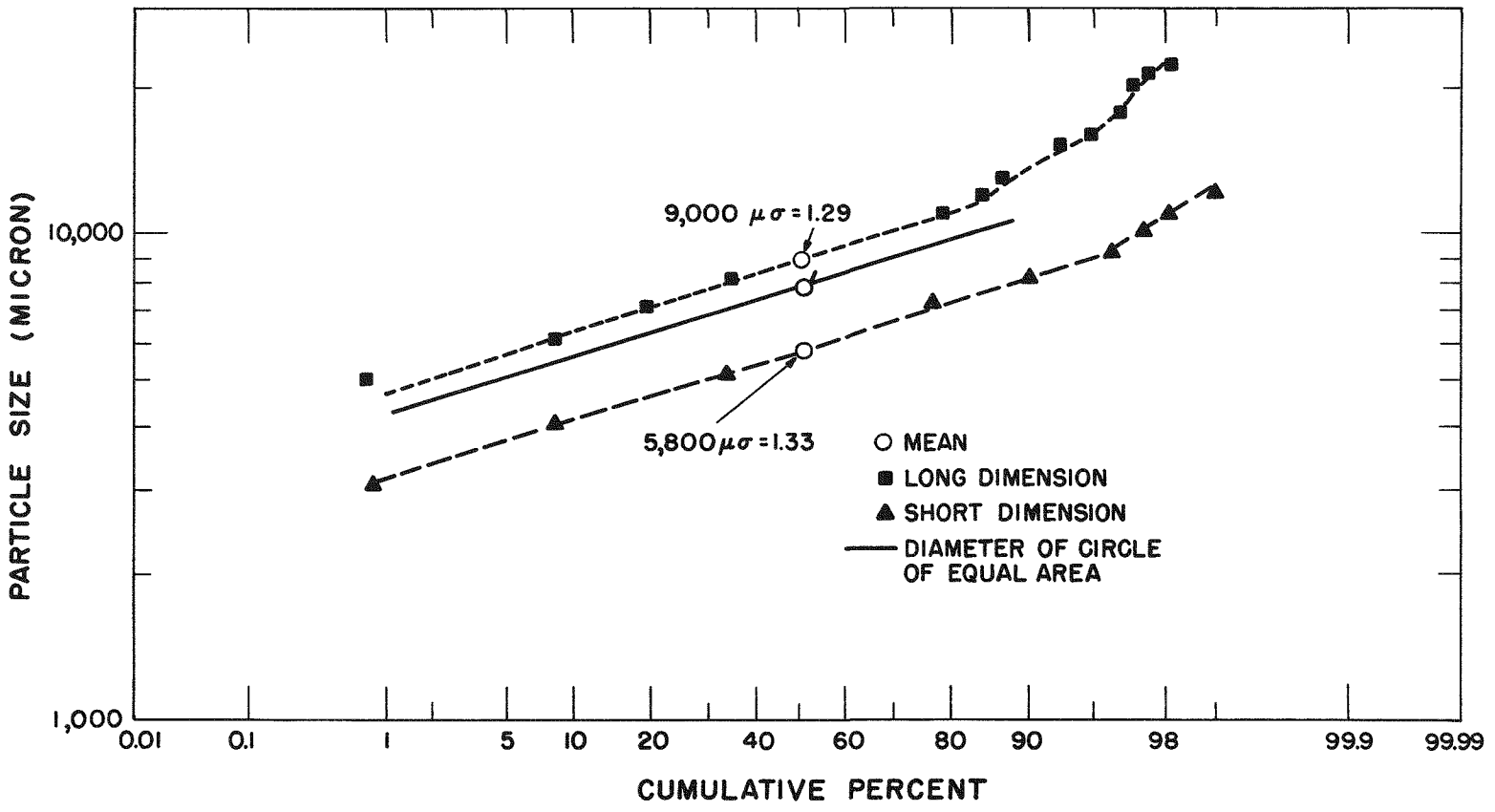

Fig. 11. Distribution of particle dimensions. Particles > 5000 μ.

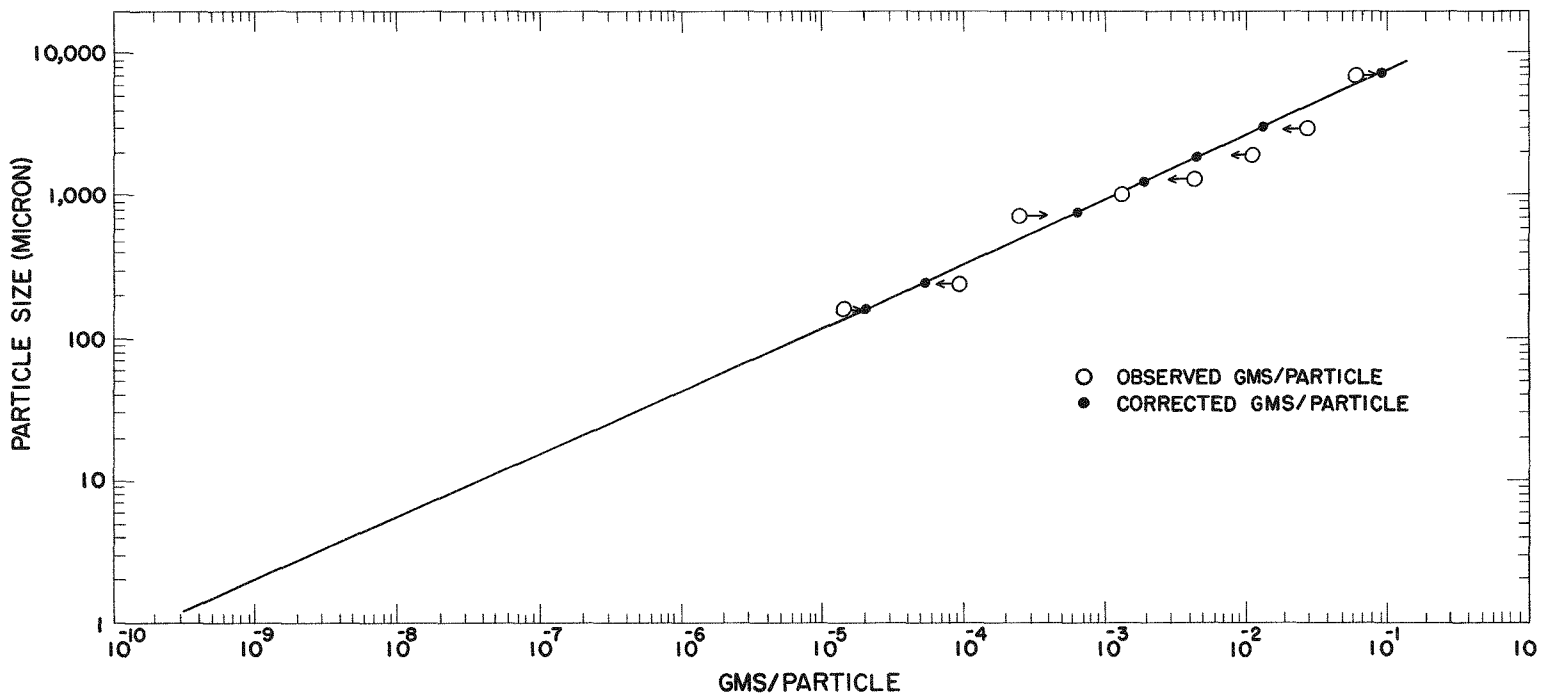

Fig. 12. Weight of single particle vs. measured diameter.

CONFIDENTIAL

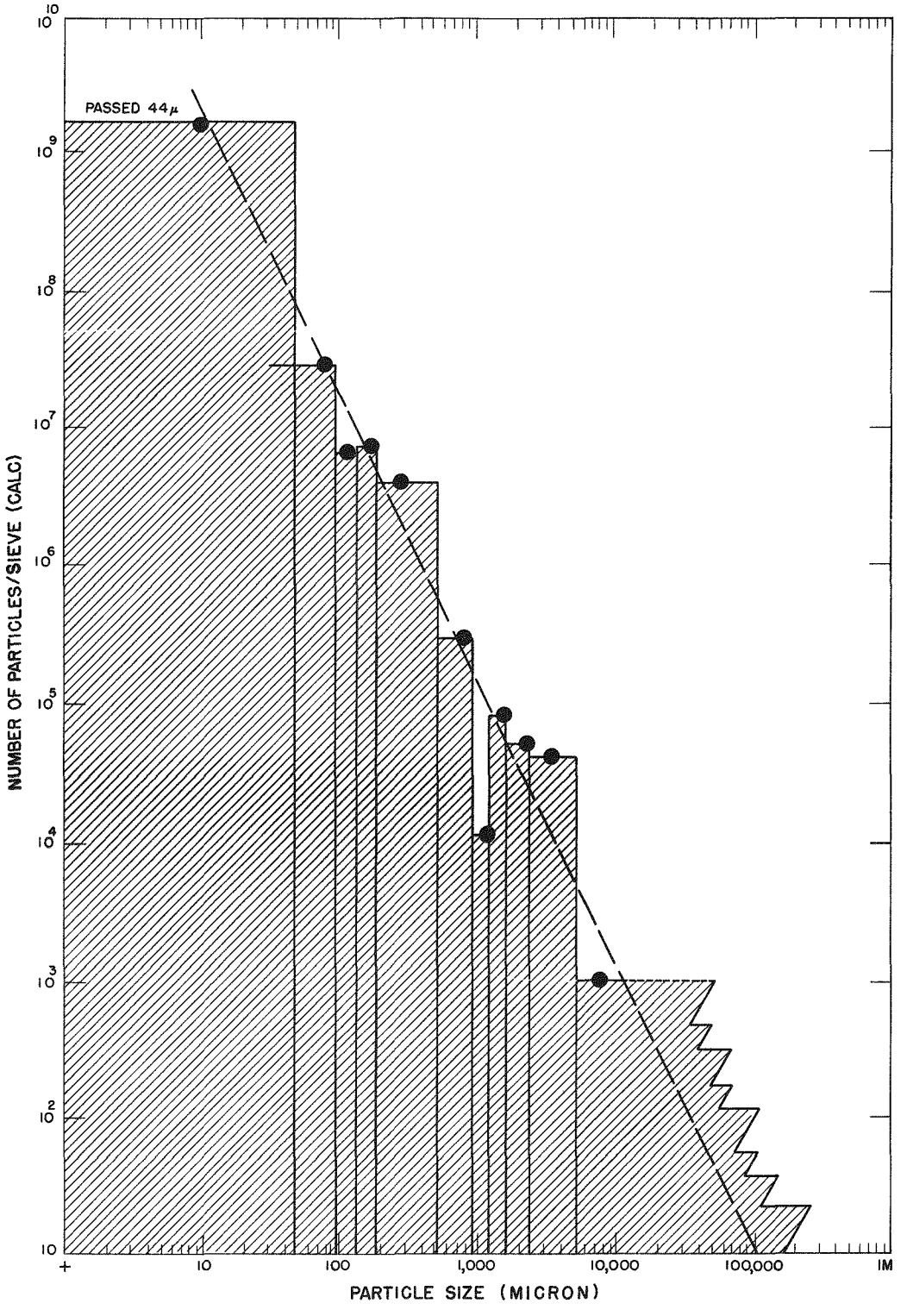

Fig. 13. Number of particles in each sieve range.

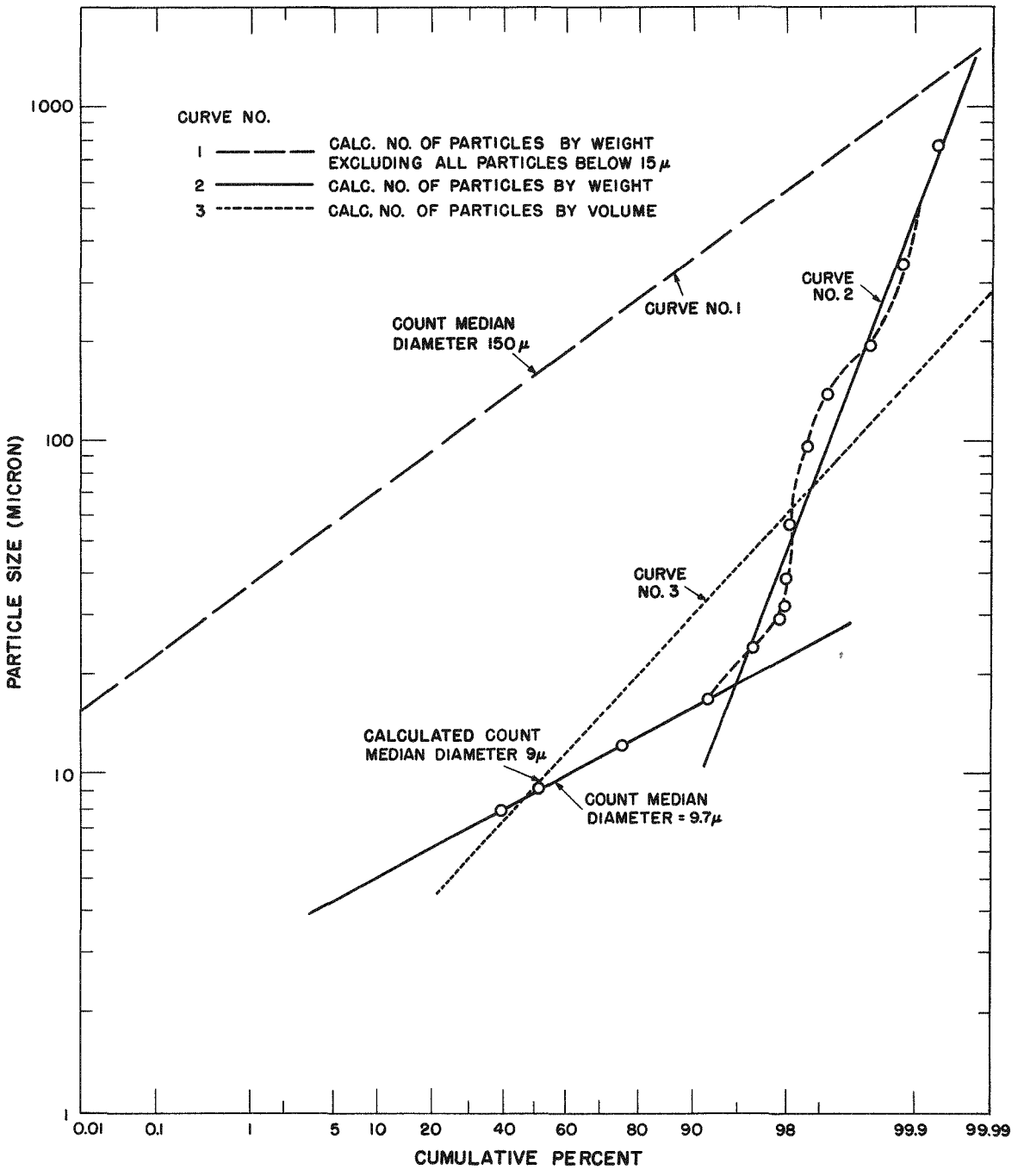

Fig. 14. Size distribution by number of particles.

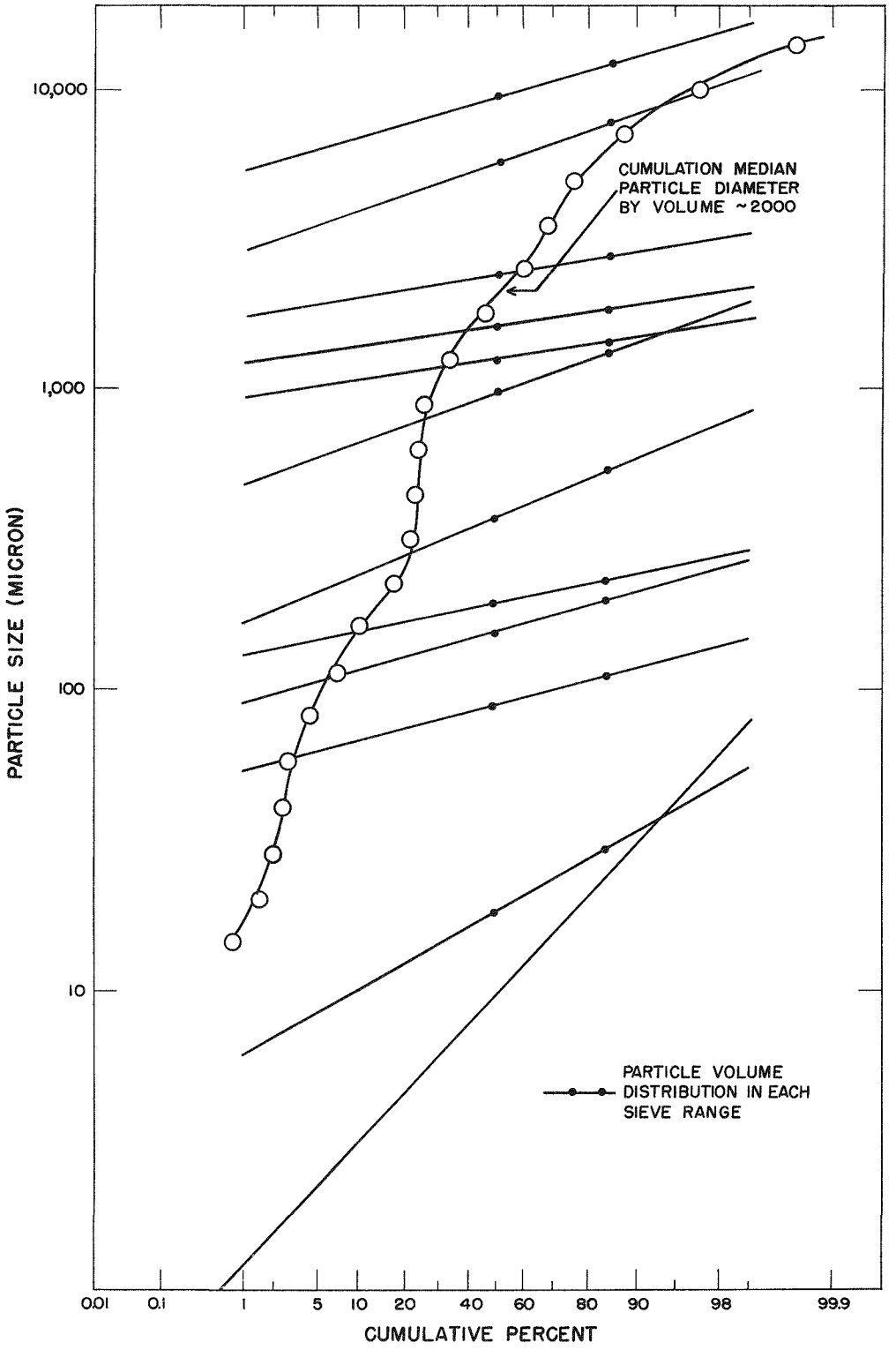

Fig. 15. Particle distribution by volume.

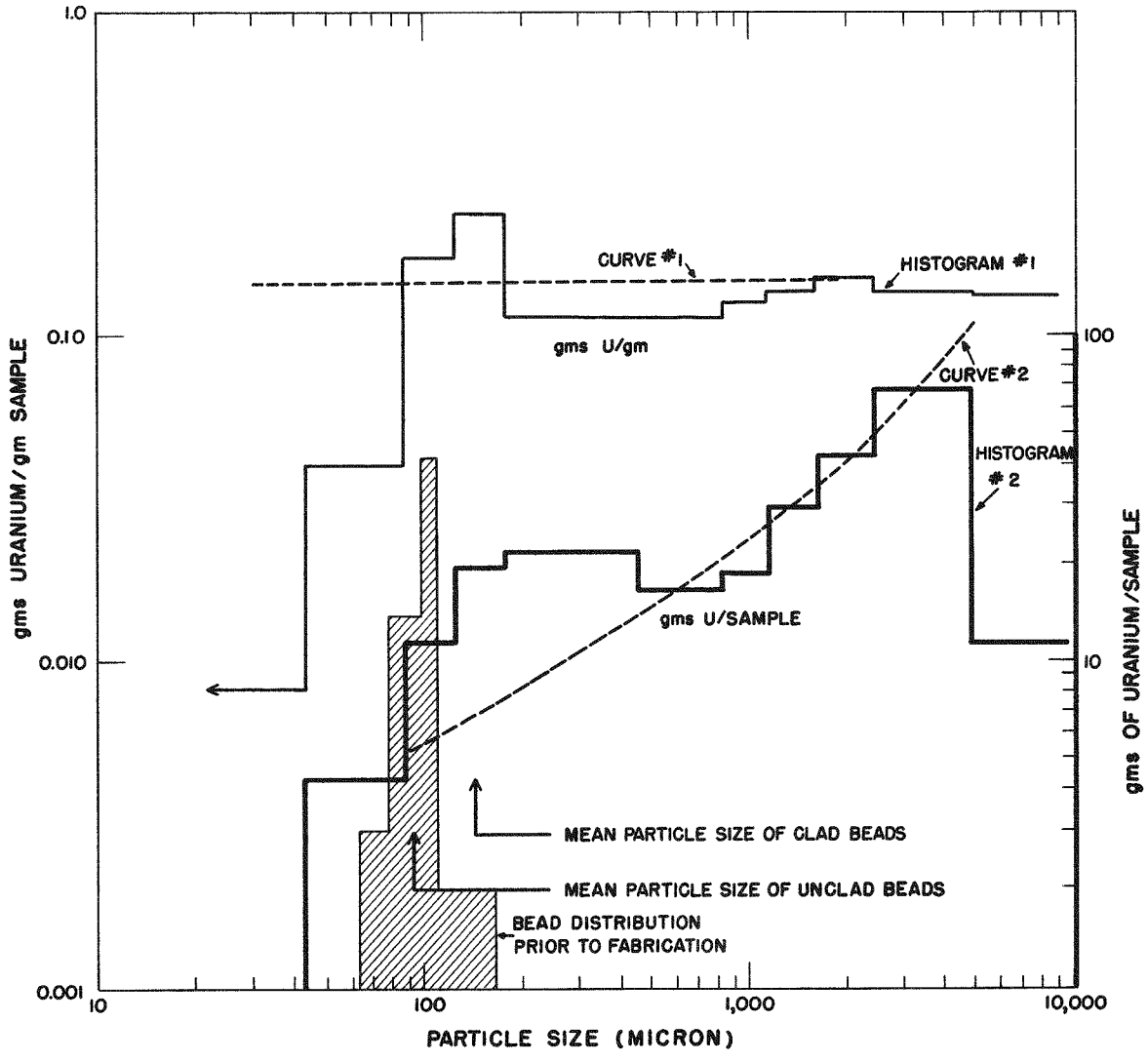

Fig. 16. Distribution of uranium by particle size fractions.

CONFIDENTIAL

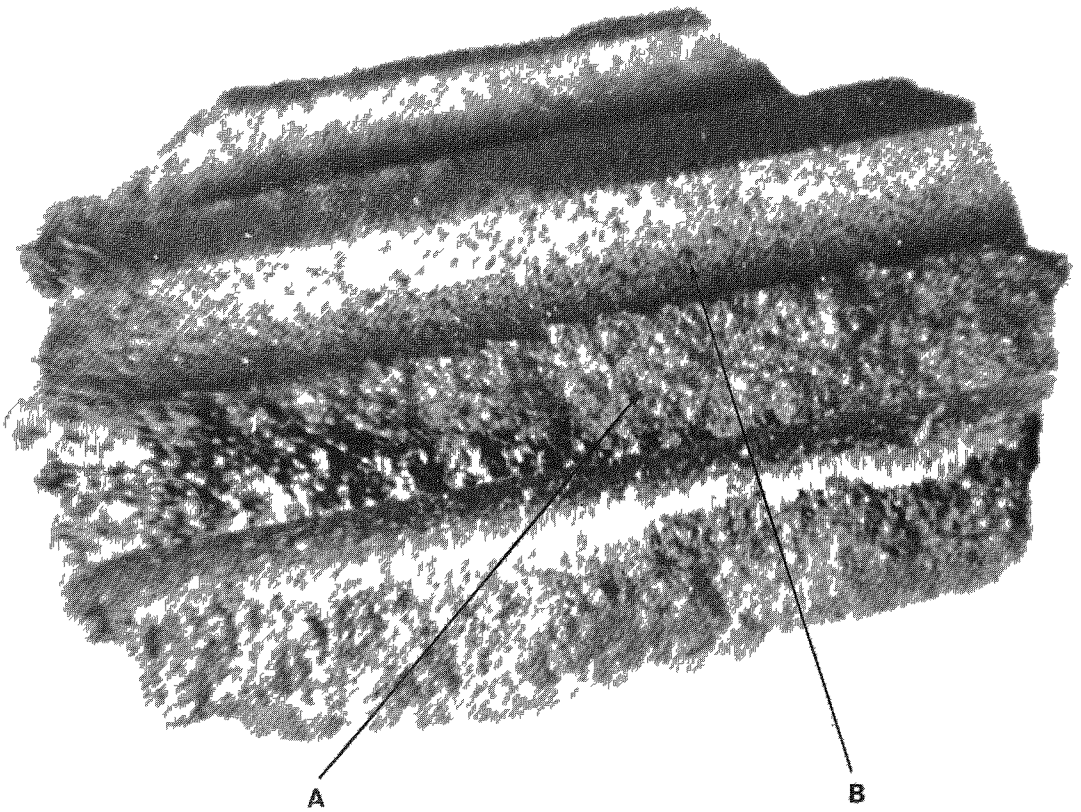

Fig. 17. Surface characteristics of a particle.

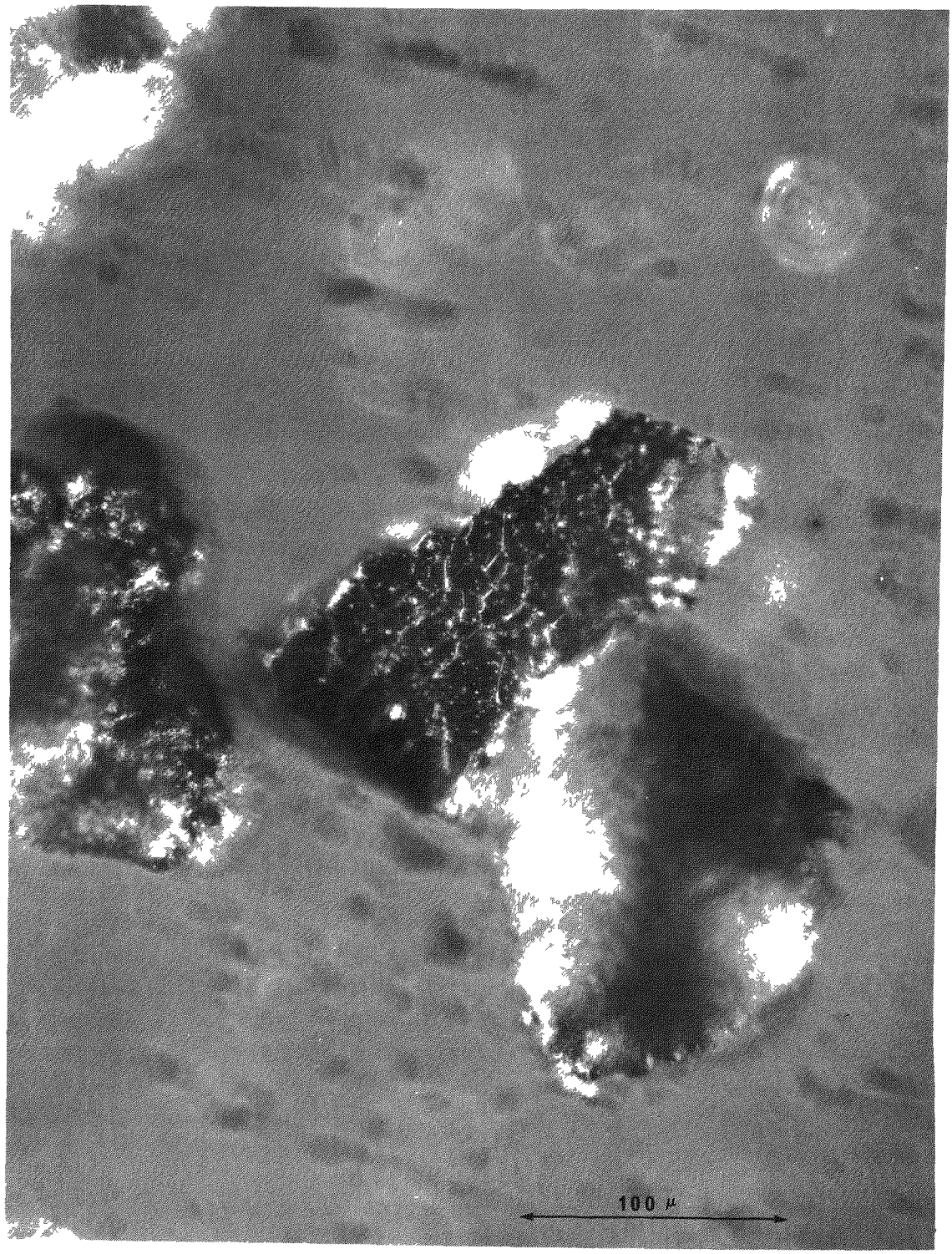

Fig. 18. Sieved sample. 125 to 177 μ.

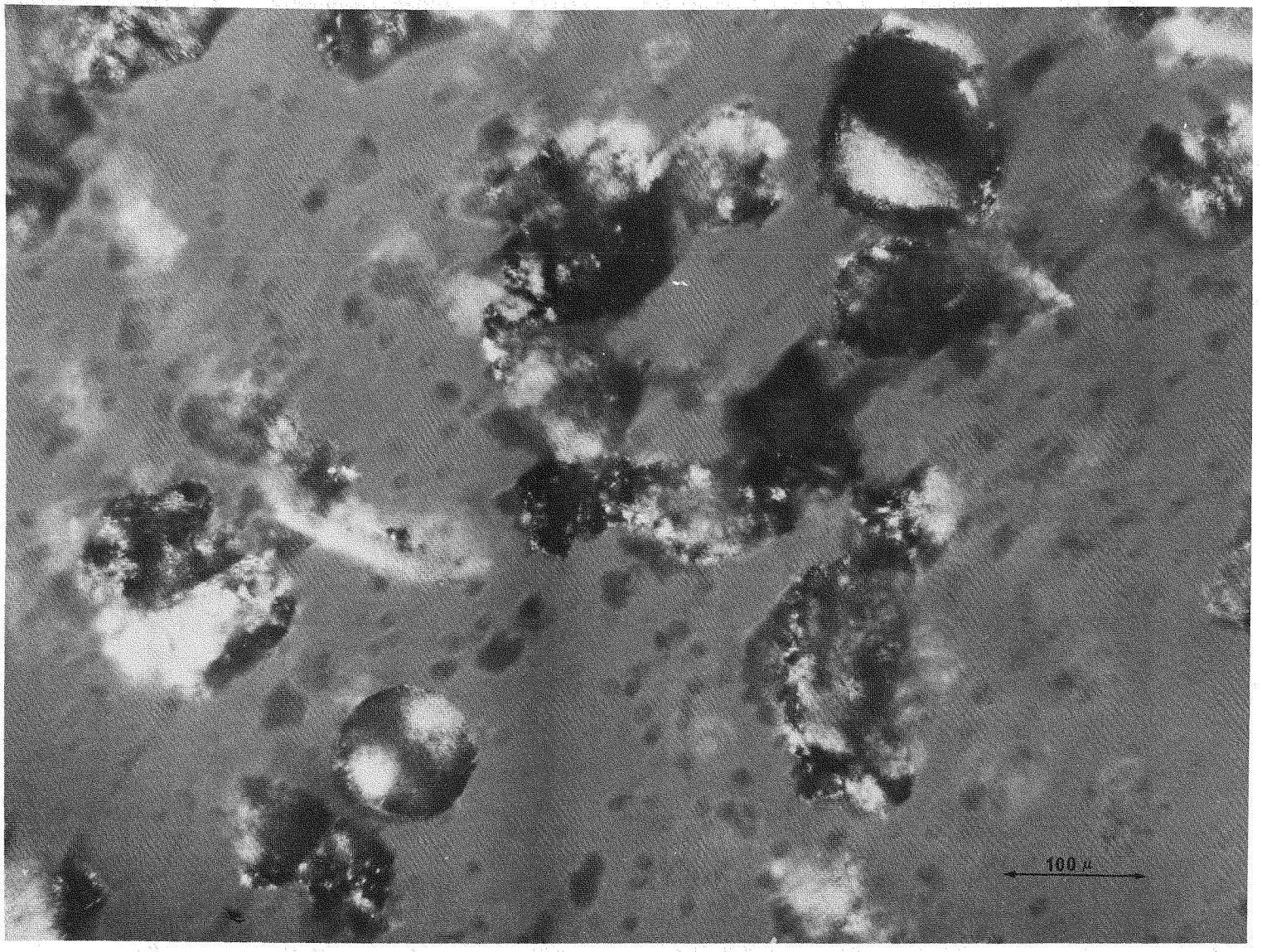

Fig. 19. Sieved sample. 88 to 125 μ.

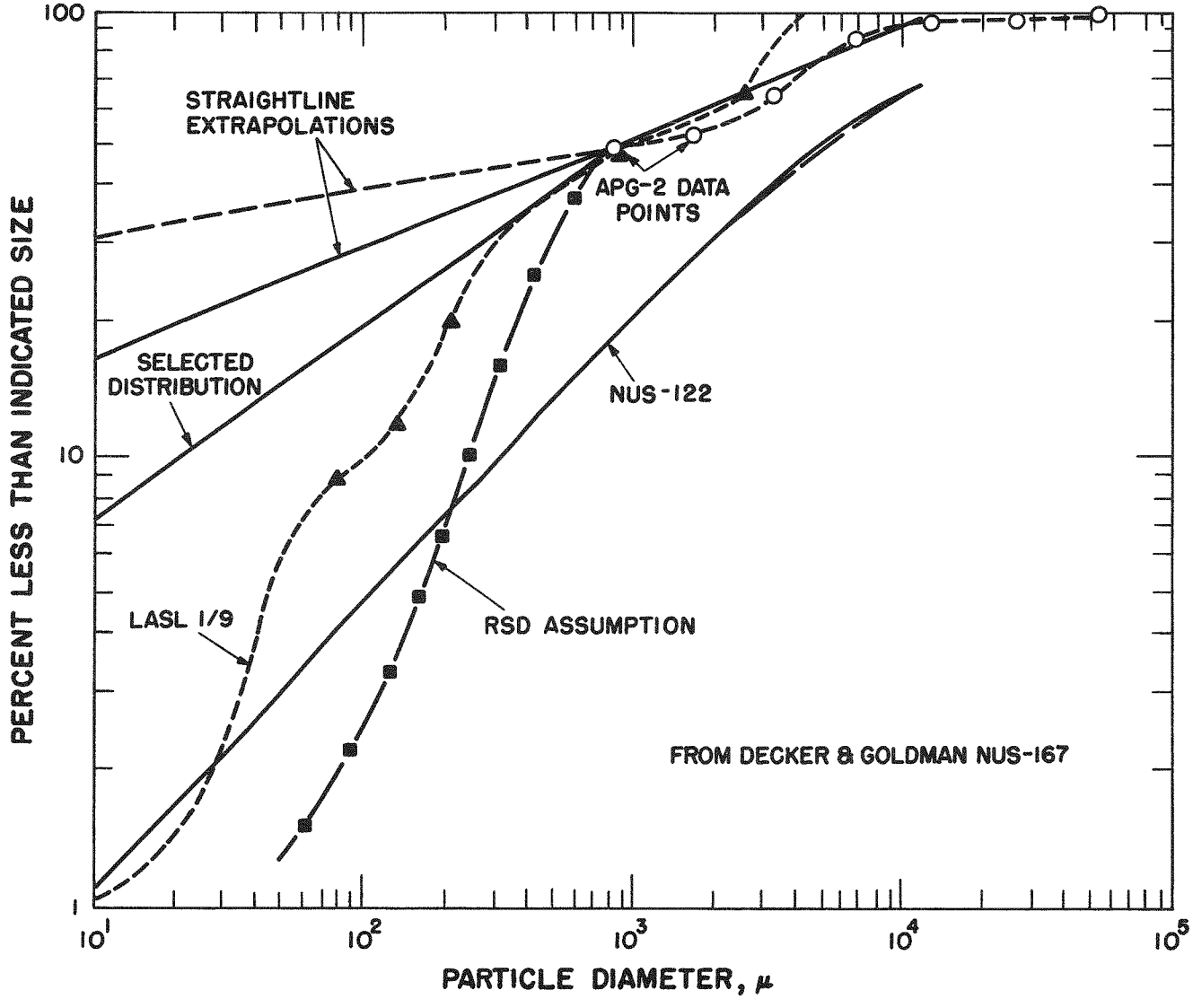

Fig. 20. Particle size distribution.